Journal of Hydraulic Research

ISSN: 0022-1686 (Print) 1814-2079 (Online) Journal homepage: http://www.tandfonline.com/loi/tjhr20

A study of flow dynamics and implications for benthic fauna in a meander bend of a lowland river

Alexander N. Sukhodolov, Martin Blettler, Jingxin Zhang, Tatiana Sukhodolova & Gunnar Nützmann

To cite this article: Alexander N. Sukhodolov, Martin Blettler, Jingxin Zhang, Tatiana Sukhodolova & Gunnar Nützmann (2015) A study of flow dynamics and implications for benthic fauna in a meander bend of a lowland river, Journal of Hydraulic Research, 53:4, 488-504, DOI: 10.1080/00221686.2015.1055598

To link to this article: http://dx.doi.org/10.1080/00221686.2015.1055598

Published online: 21 Aug 2015.

Journal of Hydraulic Research Vol. 53, No. 4 (2015), pp. 488–504
http://dx.doi.org/10.1080/00221686.2015.1055598

Research paper

A study of flow dynamics and implications for benthic fauna in a meander bend of a lowland river

ALEXANDER N. SUKHODOLOV (IAHR Member), Senior Scientist, *Department of Ecohydrology, Leibniz-Institute of Freshwater Ecology and Inland Fisheries, Berlin, Germany*
Email: alex@igb-berlin.de (author for correspondence)

MARTIN BLETTLER, Scientist, *Ciudad Universitaria, National Institute of Limnology (INALI), Hydro-Geo-Ecology Research Group, Santa Fe, Argentina*
Email: martinblettler@hotmail.com

JINGXIN ZHANG, Associate Professor, *Shanghai Jiao Tong University, School of Naval Architecture, Ocean and Civil Engineering, Department of Engineering Mechanics, Shanghai, People's Republic of China*
Email: zhangjingxin@sjtu.edu.cn

TATIANA SUKHODOLOVA, Scientist, *Department of Ecohydrology, Leibniz-Institute of Freshwater Ecology and Inland Fisheries, Berlin, Germany*
Email: suhodolova@igb-berlin.de

GUNNAR NÜTZMANN, Professor, *Department of Ecohydrology, Leibniz-Institute of Freshwater Ecology and Inland Fisheries, Berlin, Germany*
Email: nuetzmann@igb-berlin.de

ABSTRACT
Channel curvature and riffle-pool bathymetry in meandering streams control complex hydrodynamic and morphodynamic processes. This study investigates how spatial and temporal heterogeneities in flow hydraulics influence benthic fauna in a meander bend of a lowland sand-bed river. Spatial heterogeneity of riverbed morphology and secondary flow, induced by channel curvature, make pools hydraulically more diverse compared with riffles. Numerical simulations demonstrate that velocity reversal between riffles and pools in this meander bend produces spatially variable flow with complex temporal variations. Patterns of macro-invertebrates indicate an increase in population density from riffle to pool, reflecting an increase in diversity of abiotic factors. For most invertebrate species the observed patterns persisted during temporal variations of the flow. Considerable changes were observed only in some groups with specific preferences.

Keywords: Benthic fauna; eco-hydraulics; invertebrates; meander bend; turbulence

1 Introduction

The planform of natural streams commonly features a winding pattern composed of meander bends – meso-forms of alluvial channels regarded as elementary geomorphological units (Leopold, 1996). Longitudinal profiles of the riverbed thalweg in meanders composed of topographic highs (riffles) and lows (pools) the position of which corresponds to bend inflections and apices, respectively (Leopold, 1996; Rozovskii, 1957). Fluvial hydraulics research has traditionally focused on the effects of planform curvature on the flow structure and on the interaction between morphodynamics processes (Abad & García, 2009; Blanckaert & de Vriend, 2003; Engel & Rhoads, 2012; Ippen, Drinker, Jobin, & Shemdin, 1962; Rhoads & Massey, 2012; Rozovskii, 1957; Stølum, 1998). Recently, river meanders have been viewed as an intrinsic part of fluvial ecosystems (Blettler, Amsler, Ezcurra de Drago, & Marchese, 2008; Doledec, Lamouroux, Fuchs, & Merigoux, 2007; Kawamura, Hasegawa, & Yuping, 2003; Rempel, Richard, & Healey, 2000). Reconstruction of channel sinuosity is a common practice in modern

Received 16 August 2013; accepted 24 May 2015/Open for discussion until 29 February 2016.

ISSN 0022-1686 print/ISSN 1814-2079 online
http://www.tandfonline.com

river management and ecosystem restoration. Despite this past work, it is widely acknowledged that complex relations between the flow dynamics, morphodynamics and aquatic organisms in meandering rivers are insufficiently understood.

Flow through a meander bend is influenced by centrifugal force induced by channel curvature that produces a cross-stream pressure gradient that drives secondary flow (Abad & García, 2009; Rhoads, & Massey, 2012; Rozovskii, 1957). A small counter-rotating helical cell often forms near the surface at the outer bank and the three-dimensional topography of the free surface can generate flow stagnation along the outer bank at the entrance to the bend (Blanckaert & de Vriend, 2003; Ippen et al., 1962). Bars on the inside of the bends induce topographical steering (Dietrich & Smith, 1983) and recent field studies indicate that riffle-pool sequences in the meander bends can strongly modify the vertical profiles of mean velocity and turbulent shear stress distributions (Schnauder & Sukhodolov, 2012; Sukhodolov, 2012). Moreover, migrating bedforms can modulate the flow structure in meandering channels (Abad, Frias, Garcia, & Buscaglia, 2013).

High and low flow events further complicate spatially variable flow in meander bends by imposing temporal variations. Since the seminal observations by Seddon on the Mississippi River in 1900, it has been hypothesized that a reversal of hydraulic conditions may occur in riffle-pool sequences (Keller & Florsheim, 1993). This hypothesis, known as velocity reversal, proposes that flow velocities are maximal in riffles and minimal in pools during low flow events, but that the situation reverses during high flow events with maximal velocities in pools and minimal velocities in riffles (Keller, 1971; Keller & Florsheim, 1993; MacWilliams, Wheaton, Pasternack, Street, & Kitanidis, 2006). Keller (1971) used this hypothesis to explain the maintenance mechanisms in riffle-pool sequences.

Benthic macro-invertebrates are aquatic organisms that directly and indirectly experience interactions with flow, sediment transport and morphodynamic processes. Communities of benthic invertebrates can be considered as indicators of fluvial ecosystem state because of their sensitivity to water quality and sudden changes in the environment. For invertebrate communities, river meanders represent meso-scale habitats that are highly heterogeneous and comprised of micro-scale units called biotopes. Biotopes are spatially quasi-homogeneous areas with respect to abiotic factors such as riverbed morphology, composition of riverbed material, and flow characteristics. The concept of physical biotopes associates geomorphological features (riffles and pools) and flow patterns to abundance and composition of benthic communities, thereby providing opportunities for assessing habitat patchiness, diversity, and dynamics (Padmore, 1998; Newson & Newson, 2000).

Physical biotopes are characterized by specific hydrodynamic patterns and values of flow characteristics (Jowett, 1993; Padmore, 1997; Wadeson, 1994). Turbulent river flow affects benthic invertebrates either directly through dislodgement and abrasion or indirectly by influencing availability of food and oxygen concentrations, or by affecting predation, dispersal and reproduction (Carling, 1995; McNair, Newbold, & Hart, 1997; Powers & Kittinger, 2002; Quinn & Hickey, 1994). Benthic micro-habitats with strong flow or high levels of turbulence provide refuge for some invertebrate species. In such habitats predators experience larger hydrodynamic forces than prey because predators are bigger in size and project further above the riverbed than prey (Hart & Merz, 1998). Because of such factors, the success of hunting can be significantly reduced (Malmqvist & Sackmann, 1996). Gibbins, Verticat, & Batulla (2007) report that the total number of individuals lost from the riverbed and the taxonomic composition of the drift are strongly influenced by shear stress and mobility of the riverbed. Experiments examining drift of caddisfly larvae have indicated that drift distance is inversely related to the roughness of the riverbed (Holomuzki & van Loan, 2002). Drift propensity was significantly related to Reynolds and Shields numbers and hydraulically rough riverbeds are more favourable to benthic invertebrates (Wilcox, Peckarsky, Taylor, & Encalada, 2008). However, habitat preferences in invertebrates vary during the ontogenesis (Sagnes, Merigoux, & Peru, 2008). Within the same invertebrate species larval and adult organisms demonstrate different preferences for flow velocity (Degani et al., 1993; Lloyd & Sites, 2000).

The dynamics of benthic invertebrate communities in meandering rivers under variable hydraulic conditions remain poorly understood. Furthermore, knowledge of turbulent flow in meander bends of natural rivers is still incomplete. Interactions among effects induced by centrifugal acceleration, flow stagnation, and topographical steering complicate quantitative predictions of flow patterns (Abad & García, 2009; Stølum, 1998; Zeng, Constantinescu, Blanckaert, & Weber, 2008). Knowledge of these patterns is mainly acquired by experimental research involving physical models and theoretical approaches (Blanckaert & de Vriend, 2003; Engelund, 1974; Rozovskii, 1957). However, laboratory models typically lack the longitudinal variability in flow depth characteristic of natural riffle-pool sequences (Sukhodolov, 2012). The problem of scale further complicates the situation. Most field studies have been carried out in relatively small rivers (Anwar, 1986; Bathurst, Thorne, & Hey, 1979; Dietrich & Smith, 1983; Engel & Rhoads, 2012; Frothingham & Rhoads, 2003; Nanson, 2010; Thorne et al., 1985) and a handful of investigators have examined flow in large meandering rivers (Jackson, 1975; Rozovskii, 1957; Schnauder & Sukhodolov, 2012; Sukhodolov, 2012). Moreover, the velocity reversal phenomenon may not be a characteristic feature for all riffle-pool sequences (Bathurst, 1982; Rodríguez, García & García, 2013; Sear, 1996; Teleki, 1972).

This study examines how changes in spatial and temporal attributes of flow hydraulics in meander bends on a relatively large river influence the density of benthic macro-invertebrate communities. In particular, it explores how flow varies spatially between pools and riffles, how the relation between flow

in pools and riffles changes with flow stage, and the relation of these changes in flow conditions to the macro-invertebrates communities. To address these issues, ideally sampling of flow, morphodynamics, and benthic organisms would occur together for a wide range of flows. However, flow conditions in particular are difficult to measure in detail at high flow. Numerical modelling calibrated against field measurements provides the basis for extending the analysis to a range of flow conditions beyond those measured directly in the field.

2 Methodology and theoretical background

In this section we first introduce the analytical framework for representation of field data and then present details of the numerical method employed in this study.

2.1 *Analytical framework*

Momentum equations for turbulent flow in a wide river meander bend are conventionally presented in a curvilinear system with r (radial), θ (tangential), and z (vertical) coordinates (Rozovskii, 1957):

$$u_r\frac{\partial u_r}{\partial r}+\frac{u_\theta}{R}\frac{\partial u_r}{\partial \theta}+w\frac{\partial u_r}{\partial z}-\frac{u_\theta^2}{R}=-gS_r+\frac{1}{\rho}\frac{\partial \tau_{rz}}{\partial z} \quad (1)$$

$$u_r\frac{\partial u_\theta}{\partial r}+\frac{u_\theta}{R}\frac{\partial u_\theta}{\partial \theta}+w\frac{\partial u_\theta}{\partial z}+\frac{u_r u_\theta}{R}=gS_\theta+\frac{1}{\rho}\frac{\partial \tau_{\theta z}}{\partial z} \quad (2)$$

where g is specific gravity, u_r, u_θ and w are radial, tangential, and vertical time-mean velocities at a point, R is radius of curvature, S_r, S_θ are radial and tangential slopes of the water surface, $\tau_{\theta z}=-\rho\overline{u'_\theta w'}$ and $\tau_{rz}=-\rho\overline{u'_r w'}$ are turbulent shear stress components where the overbar denotes the time averaging operator over time, u'_θ, u'_r and w' are velocity fluctuations in the streamwise, transverse and vertical directions, respectively, and ρ is density of water. Equations (1) and (2) together with the continuity equation after integration yield a modified relation for the bed shear stress (Sukhodolov, 2012):

$$\tau_0=\rho u_*^2=\rho g\delta_0(S_\theta-S_r) \quad (3)$$

where u_* is shear velocity, $\delta_0=(h\pm\Delta h)/\vartheta$ is a modified characteristic length scale, h is flow depth, Δh is an additional hydrodynamic pressure head due to secondary currents and topographical steering, and ϑ is a dimensionless coefficient. For a uniform flow with $\delta_0\approx h$, and $S_r=0$, Eq. (3) equals the well-known relation $\tau_0=\rho u_*^2=\rho ghS_\theta$. Vertical distribution of the total shear stress $\tau_{\theta z}+T_{\theta z}$ in meander bend with a pronounced riffle-pool sequence of riverbed is shown to obey (Sukhodolov, 2012):

$$\frac{\tau_{\theta z}+T_{\theta z}}{\rho u_*^2}=-\frac{\overline{u'_\theta w'}}{u_*^2}+F\approx 1-\eta+\frac{2w}{\kappa u_*}\exp\left(-\frac{\eta_0^2}{2\pi}\right) \quad (4)$$

where F is normalized vertical flux, $T_{\theta z}$ is advective momentum flux, w is mean vertical velocity, $\eta=z/h$ and $\eta_0=(z-\delta_0)/h$ are normalized distances from the riverbed, and $\kappa=0.41$ is the von Kármán constant. For a uniform flow, the term with the exponent in Eq. (4) becomes negligibly small and the resulting distribution of turbulent shear stress is linear.

For a uniform flow relating turbulent shear stress $-\rho\overline{u'_\theta w'}=1-\eta$ to mean flow velocity by parabolic distribution of eddy viscosity, $\nu_t=\kappa u_* z\sqrt{1-z/h}$ yields a logarithmic law:

$$\frac{u_\theta}{u_*}=\frac{1}{\kappa}\ln\left(\frac{z}{z_0}\right) \quad (5)$$

where z_0 is a hydrodynamic roughness parameter. Because secondary currents transport tangential mean momentum downward, the profile of a mean tangential velocity exhibits a submergence of the velocity maxima, which can be approximated by a modified logarithmic law (Termini & Greco, 2006):

$$\frac{u-\bar{u}}{u_*}=\frac{1}{\kappa}\sqrt{\frac{\delta}{h}}\left[\left(\frac{\delta}{h}\right)^2-\frac{\delta}{h}\ln\frac{\delta}{h}+\ln\left(\frac{z}{\delta}\right)\left(\left(\frac{1-\mathrm{sign}\,(z-\delta)}{2}\right)-\frac{\delta}{h}\left(\frac{1+\mathrm{sign}\,(z-\delta)}{2}\right)\right)\right] \quad (6)$$

where $\bar{u}$ is depth-averaged velocity at a vertical, and δ is a length scale characterizing submergence of the velocity maximum. Equation (6) reduces to the conventional logarithmic law, Eq. (5), when $\delta=h$.

2.2 *Numerical model*

In this study, we applied a three-dimensional numerical model of turbulent flow using an in-house code based on the finite volume method (FVM), which uses the semi-implicit schemes of discretization (Zhang, Liu, & Xue, 2006). An advantage of this model is that it allows the treatment of flow in both hydrostatic and hydrodynamic approximations. Furthermore, it was anticipated that the model might perform better for the description of flow with non-linear distribution of turbulent shear stress, which can be viewed as a consequence of the non-hydrostatic behaviour.

The governing equations of the model are given below:

$$\frac{\partial q_x}{\partial t}+\frac{\partial q_x u}{\partial x}+\frac{\partial q_x v}{\partial y}+\frac{\partial q_x\tilde{\omega}}{\partial \sigma}=-gh\frac{\partial \zeta}{\partial x}+f\,q_y+\frac{\partial}{\partial x}\left(2\upsilon_{tH}\frac{\partial q_x}{\partial x}\right)+\frac{\partial}{\partial y}\left(\upsilon_{tH}\left(\frac{\partial q_x}{\partial y}+\frac{\partial q_y}{\partial x}\right)\right)+\frac{1}{h}\frac{\partial}{\partial \sigma}\left(\frac{\upsilon_{tV}}{h}\frac{\partial q_x}{\partial \sigma}\right) \quad (7)$$

$$\frac{\partial q_y}{\partial t}+\frac{\partial q_y u}{\partial x}+\frac{\partial q_y v}{\partial y}+\frac{\partial q_y \tilde{\omega}}{\partial \sigma} = -gh\frac{\partial \zeta}{\partial x}+f\,q_x+\frac{\partial}{\partial x}\left(\upsilon_{tH}\left(\frac{\partial q_y}{\partial x}+\frac{\partial q_x}{\partial y}\right)\right) + \frac{\partial}{\partial y}\left(2\upsilon_{tH}\frac{\partial q_y}{\partial y}\right)+\frac{1}{h}\frac{\partial}{\partial \sigma}\left(\frac{\upsilon_{tV}}{h}\frac{\partial q_y}{\partial \sigma}\right) \quad (8)$$

$$\tilde{\omega}=\frac{w}{h}-\frac{u}{h}\left(\sigma\frac{\partial h}{\partial x}+\frac{\partial \zeta}{\partial x}\right)-\frac{v}{h}\left(\sigma\frac{\partial h}{\partial y}+\frac{\partial \zeta}{\partial y}\right) -\frac{1}{h}\left(\sigma\frac{\partial h}{\partial t}+\frac{\partial \zeta}{\partial t}\right) \quad (9)$$

$$\frac{\partial \zeta}{\partial t}+\frac{\partial q_x}{\partial x}+\frac{\partial q_y}{\partial y}+\frac{\partial q_\sigma}{\partial \sigma}=0,\quad \sigma=\frac{z-\zeta}{h},\ \sigma\in[-1,0] \quad (10)$$

where $q_x = hu$, $q_y = hv$, $q_\sigma = h\tilde{\omega}$ are unit discharges, u, v, and w are mean velocities in streamwise x, transverse y, and vertical z directions, $\tilde{\omega}$ is transformed vertical velocity ($\tilde{\omega}_{\sigma=0} = \tilde{\omega}_{\sigma=-1} = 0$), ζ is water level, υ_{tH} and υ_{tV} are horizontal and vertical eddy viscosity coefficients, and σ is transformed vertical coordinate.

The model (7)–(10) requires a turbulence closure scheme, which is provided by relations for the eddy viscosity coefficients. The horizontal eddy viscosity is determined by a Smagorinsky-type formulation, which accounts for the horizontal resolution of the computational grid and velocity gradients:

$$\upsilon_{tH}=c_h\,\Delta x\,\Delta y\left[\left(\frac{\partial u}{\partial x}\right)^2+0.5\left(\frac{\partial v}{\partial x}+\frac{\partial u}{\partial y}\right)^2\right]^{1/2} \quad (11)$$

where c_h is an arbitrary Smagorinsky parameter varying from 0.01 to 0.5 (Blumberg & Mellor, 1983; Davies, Jones & Xing, 1997; Zhang & Chan, 2003). The vertical eddy viscosity is defined as:

$$\upsilon_{tV}=\tilde{\upsilon}f_{v1},\ f_{v1}=\frac{\chi^3}{\chi^3+c_{v1}^3},\ \chi=\frac{\tilde{\upsilon}}{\upsilon} \quad (12)$$

and it is determined by solving the one-equation Spalart-Allmaras model (Spalart, 2000) for $\tilde{\upsilon}$

$$\frac{\mathrm{D}\,\tilde{\upsilon}}{\mathrm{D}\,t}=c_{b1}\tilde{S}\,\tilde{\upsilon}-c_{w1}f_w\frac{\tilde{\upsilon}}{z}+\frac{1}{\theta}\{\nabla\cdot[(\upsilon+\tilde{\upsilon})\nabla\tilde{\upsilon}]+c_{b2}(\nabla\tilde{\upsilon})^2\} \quad (13)$$

where $f_w = G\left(\frac{1+c_{w3}^6}{g^6+c_{w3}^6}\right)^{1/6}$, $G = r + c_{w2}(r^6 - r)$, $r=\frac{\tilde{\upsilon}}{\tilde{S}\kappa^2 z^2}$, $\tilde{S}=|\bar{S}|+\frac{\tilde{\upsilon}}{\kappa^2 z^2}f_{v2}$, $\bar{S}_{ij}=\frac{1}{2}\left(\frac{\partial u_i}{\partial x_j}+\frac{\partial u_j}{\partial x_i}\right)$, $f_{v2}=1-\frac{\chi}{1+\chi f_{v1}}$, with the model constants $c_{b1} = 0.1355$, $\theta = 2/3$, $c_{b2} = 0.622$, $c_{w1} = c_{b1}/\kappa^2 + (1 + c_{b2})/\theta$, $c_{w2} = 0.3$, and $c_{v1} = 7.1$. The numerical method is based on the semi-implicit scheme (Casulli & Cattani, 1994; Chen, 2003; Zhang, Liu & Xue, 2006). The computational domain is represented by an unstructured grid and the C-C (Cell-Centred) scheme is used to array the variables into the computational cells. The cell face variable $\langle\phi\rangle^\eta$ is calculated by means of the second order TVD scheme:

$$\langle\phi\rangle^\eta=\phi_c+\frac{1}{2}\psi(r_\eta)(\phi_D-\phi_C) \quad (14)$$

where η is the cell face, ϕ_D and ϕ_C are the cell-centred variants in the downwind and upwind nodes around the face, and $\psi(r_\eta)$ is a flux limiter function. Assuming that $\psi(r_\eta)$ is a linear function of r_η, a higher order scheme can be obtained. Pressure-velocity coupling on the collocated grid is achieved with an interpolation scheme suggested by Rhie & Chow (1983).

3 Field studies

3.1 *River reach*

Field studies were carried out in the Spree River in Germany near the village of Neubrück in Brandenburg. The river reach is a typical meander bend, which was developing under pristine conditions during the pre-industrial period and later it was conserved because of alterations in the hydrologic regime of the river (Nikolaevich, Sukhodolov & Engelhardt, 2004; Sukhodolov, 2012). The meander bend is mildly curved, slightly asymmetrical in the planform with pronounced riffle and pool sections (Fig. 1b). The stability of the bend's large-scale morphology is an important feature for the design of this study in which numerical modelling is applied to the same riverbed topography at various water stages. The river bend at the study site has an arc angle of $\alpha = 150°$, path length of $S_m = 760$ m, bend wavelength of $\lambda = 485$ m, and sinuosity of $S_m/\lambda = 1.57$ (Fig. 1). At the bank-full stage the river is roughly 30–50 m wide and 3–7 m deep. The riverbed of the reach is composed of sands with a mean diameter around 1.2 mm in the central part. Near the inner bank the riverbed material is a bimodal mixture of sand with a mean diameter 1.2 and silted fine sand with a mean diameter of 0.2 mm. Although the riverbed material near the outer bank is also bimodal, its composition is different from both the central and the inner parts of the channel. The dominant fraction is gravel with a diameter of 8 mm and the interstitial spaces are filled by finer sand of 0.4 mm in diameter(Sukhodolov, 2012).

3.2 *Field measurements*

Field studies consisted of the three measuring campaigns (Table 1). A detailed bathymetric survey was completed before the measurement campaign 1. Geodetic measurements were obtained with a laser total-station and yielded a local coordinate system. Bathymetry along a set of 25 uniformly spaced cross-sections in the meander path was surveyed with a portable echosounder and referenced to the coordinate system. The survey data yielded a topographic map of the river reach that was used to determine cross-section locations for velocity measurements (Fig. 1a). The plan-form of the bend was slightly

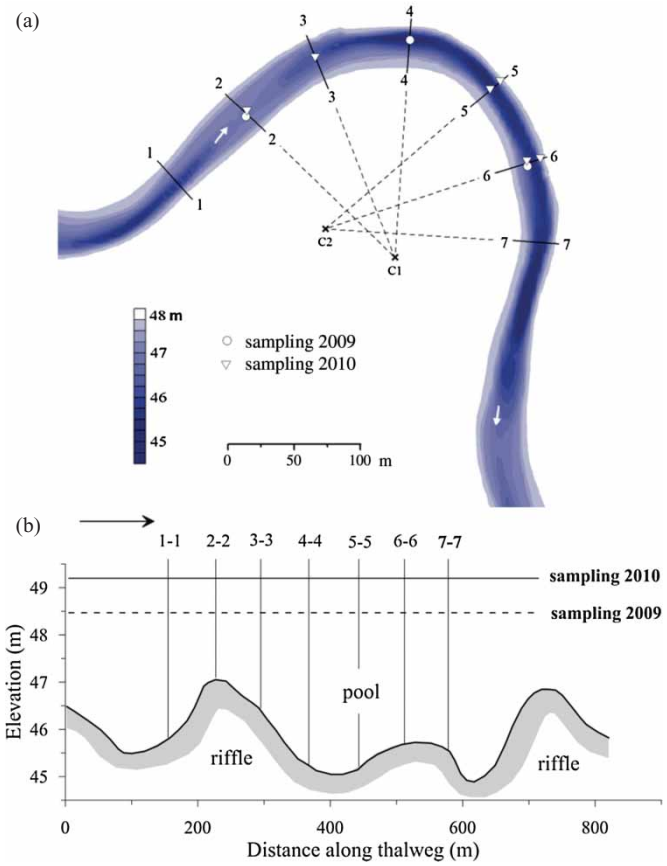

Figure 1 (a) Bathymetry map of the study reach in the Spree River (symbols indicate locations of benthic samples); (b) longitudinal profile of the riverbed and water surface elevations

asymmetric; hence, it was approximated with two segments of the same radius $R_1 = R_2 = 165$ m, but with different locations of their centres C_1, C_2. Six cross-sections were uniformly distributed along the bend path: three sections at each of the segments and one additional cross-section at the bend entrance. Each cross-section was oriented normal to the arc of curvature, thus ensuring the proper orientation of cross-sections in the system of curvilinear coordinates (1) and (2). The end positions of cross-sections were fixed in the field with iron pipe bench-marks. At each measuring cross-section three samples of riverbed material were taken near banks and in the central part of the channel.

The campaign 1 included detailed measurements of instantaneous three-dimensional flow velocities at each of seven cross-sections (Fig. 1a). An array of three ADV units, each with its own mounting mast, was used simultaneously. Correct alignment of each ADV mount and sensor head was achieved by aligning the orientation of the mount with the plane of the section by using a theodolite stationed at one of the bench-marks and siting on the other bench-mark (Sukhodolov, 2012). At each cross-section, velocities were measured at 11 locations distributed uniformly over depth at 9 to 15 verticals. The sampling period for each location was 240 s at the sampling rate of 25 Hz. Water levels were monitored at three locations: the entrance to the bend, near the apex, and at the outlet of the bend. Local depth of flow at each vertical profile was measured with a sounding rod.

The results of the first measuring campaign are presented in detail by Sukhodolov (2012). In the riffle section of the bend the structure of mean flow and turbulence is similar to that of a fully developed quasi-uniform open-channel flow in straight river reaches (Nezu & Nakagawa, 1993; Sukhodolov, 2012; Sukhodolov & Uijttewaal, 2010, see also Fig. 2a,c). The ensemble-averaged profiles of mean tangential velocity in Fig. 2a are presented in dimensionless coordinates $\xi = \exp[(u - \bar{u})\kappa/u_* - 1]$ for the riffle section, and in $\xi^* = \exp[(u - \overline{u})\kappa/u_* - f(\delta, h)]$ for the pool section (Sukhodolov, 2012). In the riffle section patterns of velocity vectors indicate an absence of helical motions characteristic of secondary currents. At the pool section, the action of centrifugal forces due to curvature results in a well-developed secondary flow with the velocity magnitude near the riverbed as large as 10–15% of the local depth-averaged velocity (Fig. 2b). Flow patterns in cross-sections downstream from the bend apex include a counter-rotating cell near the outer bank. This cell is produced by flow stagnation in cross-section 5–5 and it grows in size in

Table 1 Hydraulic characteristics during measurements

	Campaign	Q (m^3 s^{-1})	$S_\theta \times 10^5$	Riffle			Pool		
				U (m s^{-1})	u_* (cm s^{-1})	h (m)	U (m s^{-1})	u_* (cm s^{-1})	h (m)
1	detailed hydrodynamic measurements (7 cross-sections) April-May 2004	7.5	2.5	0.20	1.7	1.56	0.14	1.0	3.18
2	reduced hydrodynamic measurements (cross-section 2) June 2009	11.3	4.0	0.25	2.4	1.70	0.27*	2.3*	3.30
3	hydrometric measurements (discharge and slope) August 2010	30.0	13.0	0.47*	5.1*	2.36*	0.52*	6.9*	4.00

* indicates computed values. Shear velocity of 2.5 (cm s^{-1}) is a threshold for re-suspension of fine riverbed material according to the field tests with re-suspension chamber (Kleeberg et al., 2010)

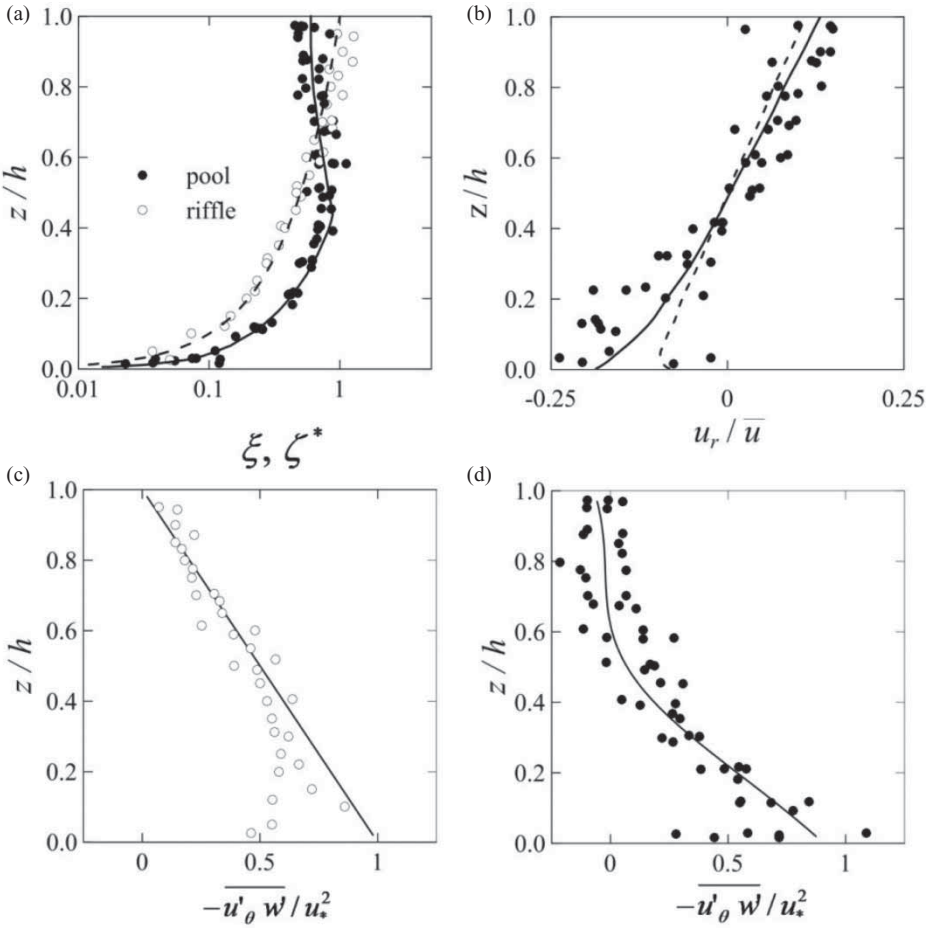

Figure 2 (a) Normalized mean tangential velocities (dashed line is logarithmic law and solid line is modified logarithmic law), (b) normalized radial velocities (dashed line is Rozovskii, 1957, profile for rough riverbed and solid line is profile for smooth riverbed), (c) shear stress profiles in riffle section (solid line is linear profile of shear stress), and (d) in pool sections (solid line is Eq. (4))

the downstream direction (cross-sections 6–6 and 7–7). The cell occupies the upper 1/3 of the water column and the strongest interactions between this cell and the main cell of the secondary flow occur near the riverbed at the outer bank (Sukhodolov, 2012). In the riffle the ensemble-averaged profiles of shear stress exhibit the structure characteristics of a fully developed uniform open-channel flow with a rough bed and the profile of turbulent shear stress $-\overline{u'_\theta w'}/u_*^2$ exhibits a linear pattern (Fig. 2c). In the pool, the ensemble-average profiles $-\overline{u'_\theta w'}/u_*^2$ scale appropriately with Eq. (4), see Fig. 2d. Shear velocity values were determined by fitting Eq. (4) to the measured profiles of turbulent shear stress and the vertical profiles of mean and turbulent flow were ensemble-averaged for riffle and pool sections. The procedure of ensemble-averaging is described in detail by Sukhodolov (2012). The values of shear velocity are summarized in Table 2. Normalized profiles of radial velocity are in agreement with the theoretical solutions by Rozovskii (1957) (Sukhodolov, 2012).

Control surveys of riverbed morphology completed in June 2009, prior to the measurement campaign 2, indicated that due to regulation of water and sediment discharges in the river at the upstream reservoir, the riverbed in the study reach had not

Table 2 Shear velocity values

	Q, (m^3 s^{-1})	Method	u_* (cm s^{-1}) in cross-sections						
			1	2	3	4	5	6	7
1	7.5	Measured	0.8	1.5	1.8	1.1	1.1	0.8	1.3
		$\sqrt{g\delta_0(S_\theta - S_r)}$	0.8	1.8	2.0	1.1	0.9	0.9	1.2
2	11.3	Measured	–	2.4	–	–	–	–	–
		$\sqrt{g\delta_0(S_\theta - S_r)}$	1.9	2.6	2.8	2.4	2.3	2.2	2.4
3	30.0	$\sqrt{g\delta_0(S_\theta - S_r)}$	5.5	5.1	5.4	5.8	6.7	6.9	6.5

changed significantly. Detailed hydrodynamic measurements were completed in the riffle section between cross-sections 2 and 3 (Fig. 1). Three vertical profiles were measured with ADVs along a centreline of the flow (Blettler, Sukhodolov & Tockner, 2010). These measurements were supplemented with the control measurements of riverbed bathymetry in the riffle (cross-section 2) and pool (cross-section 6), and monitoring the slopes of free-surface.

Campaign 3 was completed during a period of high flow in summer 2010. Although water levels in the river were below bank-full stage, the flow velocities and depths were too large for measurements with ADVs. The measurements in this campaign therefore included only control surveys of riverbed bathymetry in cross-sections 2 and 6, and reach-averaged velocity measurements with a tracer technique. The solution of uranin fluorescent dye was instantaneously injected in cross-section 1 and the travel time of the tracer cloud (as a centre of mass) was recorded with a back-scat fluorometer in cross-section 7. The slopes of the free surface were also monitored during this campaign.

3.3 *Benthic sampling*

Sampling of benthic invertebrates was performed in the second and third campaigns at 11.3 m^3 s^{-1} and 30 m^3 s^{-1} discharges (Table 1). Four replicates were taken at each sampling location, which were positioned by marked tag-lines fixed on the benchmarks of cross-sections (Fig. 1a). The invertebrate samples were collected manually by a diver who descended to the riverbed along a metal rod deployed from a boat. This method provided stabilization of the diver's position in the current and ensured the accuracy of sampling at the specific locations on the riverbed. The samples were collected manually by the diver with a Surber sampler 200 μm, and the samples were delivered to the boat where they were filtered and fixed in 90% alcohol. In total, five sampling locations were assessed at 11.3 m^3 s^{-1} water discharge, and six at 30 m^3 s^{-1}. Invertebrates were hand-picked in the laboratory under a 10 × stereoscopic microscope, identified, and stored in the solution of alcohol.

4 Results and analysis

4.1 *Validation of the numerical model*

Equations (7)–(13) are solved with three boundary conditions – inlet boundary, free surface and the boundary condition at the riverbed. The results of bathymetric surveys were used to generate a computational digital grid. An unstructured grid was composed of 24 layers in the vertical direction and every layer consists of 29,497 cells. On the inlet boundary the elevation of the free surface and the water discharge are specified. The boundary condition on the riverbed is provided by a wall function to define bed shear stress values.

Validation was completed for the hydraulic conditions of campaign 1 with $Q = 7.5$ m^3 s^{-1}. The results of validation for both primary and secondary flows are presented in Fig. 3. The results of modelling reproduce the results of measurements within an accuracy ±15–20%. The deviations are of a systematic character revealing a trend for under-prediction of velocities near the river bed and over-prediction in the upper water column near the free surface. However, due to a systematic character of deviations and the difference in their sign near the riverbed and near the free surface, cross-section averaged velocities are predicted fairly well with accuracy within ±10%.

4.2 *Modelling flow at different water stages*

Numerical modelling was performed for five water stages: 3.5, 7.5, 11.3, 30, and 50 m^3 s^{-1}, ranging from low flow to a flow slightly larger than the bank-full flow. The smallest discharge of 3.5 m^3 s^{-1} is supplied by the flow control system on this river reach and corresponds to the minimal flow required to support the aquatic ecosystem in the river. The bank-full flow of 30 m^3 s^{-1} is a rare event with a recurrence period of a decade. In contrast to rivers with a natural hydrologic regime with large discharges and relatively short durations of high-water events, floods in this river reach can last from three- to six-month periods because of continuous water releases from the upstream reservoirs.

Examples of modelled distributions of flow velocities are shown in Figs 3–6. The results of modelling demonstrate that at water discharges that do not cause inundation of the floodplain, the patterns of primary flow structure remain fairly similar and generally differ only in the magnitude of the flow (Figs 4, 5). However, in riffles the areas occupied by relatively high flow velocities increase in size with the increase of discharge. In pools, high flow velocities are localized along the outer bank of the bend (Fig. 5). The results of modelling also illustrate the influence of water stage on the secondary flow in the pool (Fig. 6). With the increasing discharge, both the magnitude of lateral and vertical velocity components and the size of secondary circulation cells increase. Although, the model does not correctly predict the near-bed velocities in the counter-rotating cell near the outer bank, it is fairly accurate in predicting velocities in the upper part of the water column. The lateral extent of the counter-rotating secondary cell is predicted fairly well and is shown to increase with the increase of discharge.

The results of numerical modelling relevant to the velocity reversal hypothesis are summarized in Fig. 7. In general, these results support the hypothesis and indicate a difference of roughly 1.2 to 1.5 fold between the magnitudes of cross-section averaged flow velocities at small and large discharges. At small discharges ($Q < 5$ m^3 s^{-1}), the velocities in the pool section are around 1.2 to 1.5 times smaller than in the riffle, while at larger discharges ($Q > 25$ m^3 s^{-1}) the velocities in the pool are around 1.3 to 1.5 times larger than in the riffle section. Shear velocities were computed according to Eq. (3) using the results of numerical modelling to determine the

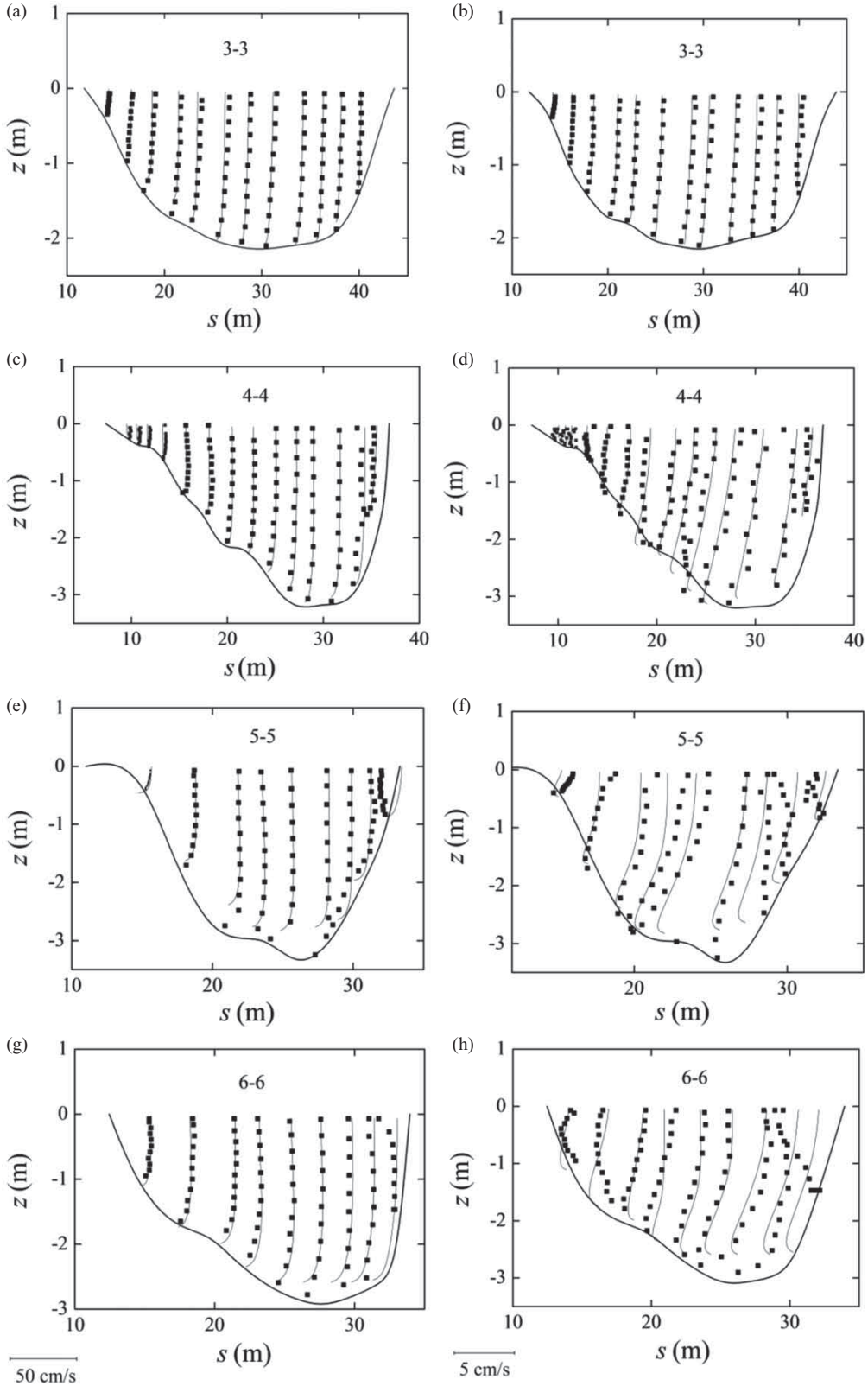

Figure 3 Comparison of measured (symbols) and modelled (solid lines) flow velocities; (a, c, e, g) are tangential velocities, and (b, d, f, h) are radial velocities

characteristic depth scale δ_0, combined with free surface slopes derived from the field measurements (Table 2). The spatial-temporal patterns of shear velocity predict that shear velocity values also reverse between pools and riffles with increasing stage. Figure 7 indicates that the first benthic sampling campaign was performed at water discharge close to the reversal point when hydraulics conditions in pools and riffles are similar. The second benthic sampling campaign was performed at

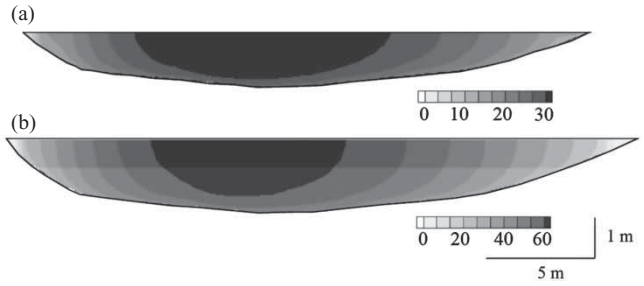

Figure 4 Modelled patterns of tangential velocity in cross-section 2-2 for (a) $Q = 11.3$ m^3 s^{-1} and (b) $Q = 30$ m^3 s^{-1} (velocity scales are in cm s^{-1})

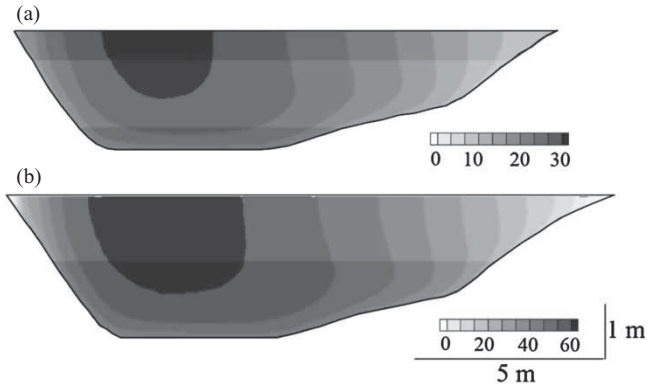

Figure 5 Modelled patterns of tangential velocity in cross-section 6-6 for (a) $Q = 11.3$ and (b) $Q = 30$ m^3 s^{-1} (velocity scales are in cm s^{-1})

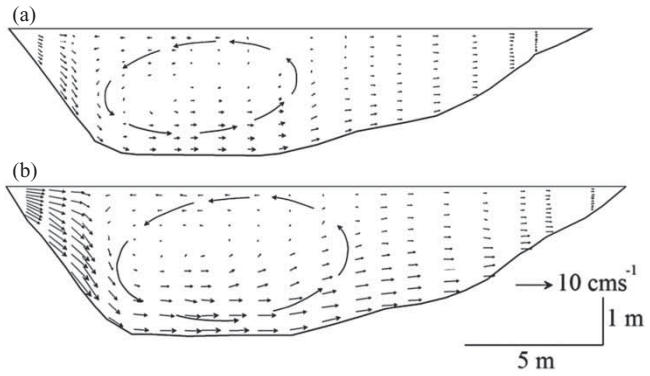

Figure 6 Modelled patterns of secondary flow in cross-section 6-6 for (a) $Q = 11.3$ m^3 s^{-1} and (b) $Q = 30$ m^3 s^{-1}

the stage of a bank-full flow when velocities in the pool section were around 30% higher than velocities in the riffle.

4.3 *Invertebrate community*

To verify the normality of the benthic data, the variables were logarithmically transformed [$\log_{10}(x+1)$] and checked for a normality within a strata (Shapiro & Wilk, 1965) as well as for a homogeneity in the variance between strata F_{max} (Sokal & Rohlf, 1981). After the normality was verified by log transformation, the parametric statistics were applied to further examine the benthic data. An ANOVA one-way test (significant differences $= p < 0.05$) was used to determine the significance of

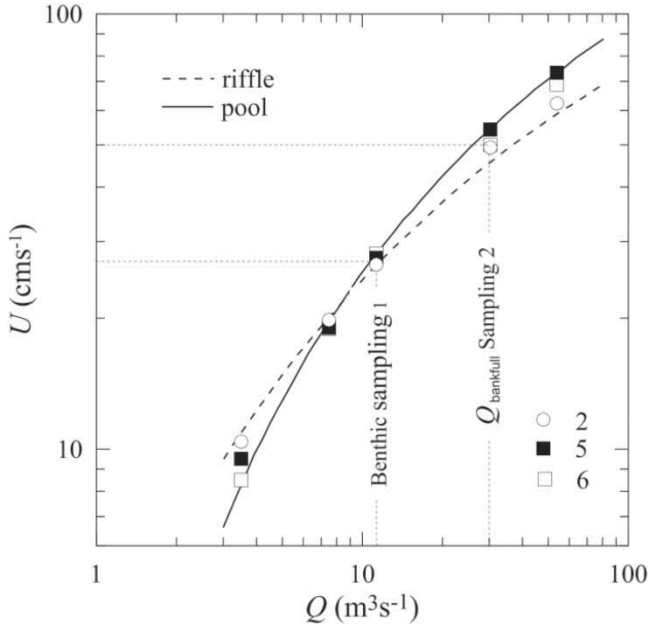

Figure 7 Variation of cross-section averaged velocity with water discharge in riffle and pool sections

differences between arithmetic means of benthic densities at each sampling location. Post-hoc, Fisher's LSD test was then used to explore differences among treatments in the ANOVA.

The main determined benthic groups were Amphipoda (*Dikerogammarus haemobaphes* (Pontogammaridae) and *Chelicorophium curvispinum* (Corophiidae)), Chironomidae (Chironomini), Naididae (Oligochaeta) and Bivalvia, the latter of which were less abundant compared with the other groups. Total population densities varied between 3.07×10^3 (cross-section 2–2, sampling 1) and 20.0×10^3 ind. m^{-2} (cross-section 5-5, sampling 2), Table 3.

The density of invertebrates was high in Sampling 2 (Q = 30 m^3 s^{-1}) compared with Sampling 1 (Q = 11.3 m^3 s^{-1}), see Fig. 8a. The results of the ANOVA analysis confirm that this difference is statistically significant (current effect: $F_{(1,30)} = 76.195$, $p = 0.000$). However, according to ANOVA results, there is no statistical difference between the population densities of Amphipoda in Sampling 1 and 2 (current effect: $F_{(1,30)} = 0.09914$, $p = 0.755$).

Chelicorophium curvispinum and *Dikerogammarus haemobaphes* (order Amphipoda) deserve to be analysed separately because of ecological differences between these species. *C. curvispinum* is an active filter feeder, one of most important primary consumers (Van der Velde et al., 1998; Van Riel et al., 2006), and prey for several species of fish (Grabowska & Grabowski, 2005) and gammarids (Van Riel et al., 2006). In contrast, *D. haemobaphes* is a predator species with a very wide ecological tolerance (Grabowski, Jazdzewski & Konopacka, 2007). Filter-feeders species, like *C. curvispinum*, prefer to occupy the microhabitats with large velocities, which support effective filter-feeding (Fuller & Mackay, 1981; Wetmore, Mackay & Newbury, 1990). This preference can explain the

Table 3 Invertebrate densities and principal benthic groups

	Invertebrate population densities (ind m^{-2})					
	Sampling 1					
Sampling stations	2–2 (1)	2–2 (2)	2–2 (3)	4–4	6–6	
Density (ind. m^{-2})	3071	4643	3364	9102	7879	
Total density (ind. m^{-2})			5611			
	Sampling 2					
Sampling stations	2–2	3–3	5–5 (middle)	5–5 (left)	7–7 (middle)	7–7 (left)
Density (ind. m^{-2})	3904	12032	12550	20000	1264	15547
Total density (ind. m^{-2})			10883			

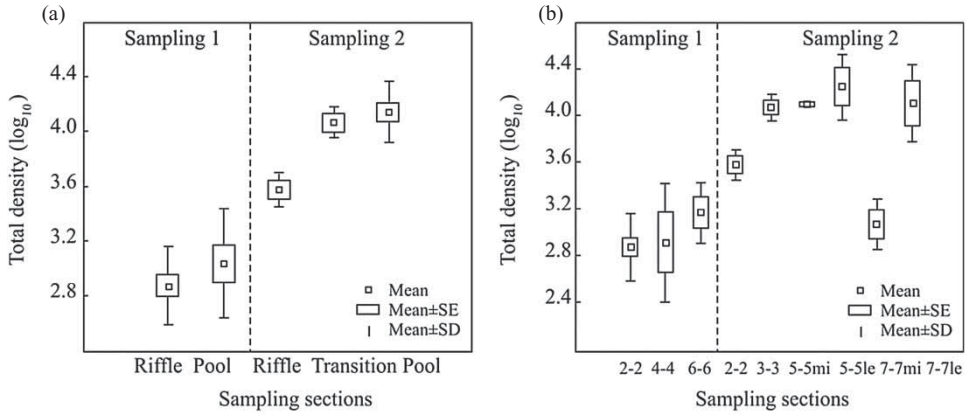

Figure 8 Patterns of total population density of micro-invertebrate in riffle, intermediate and pool sections (a), and at each sampling station (b)

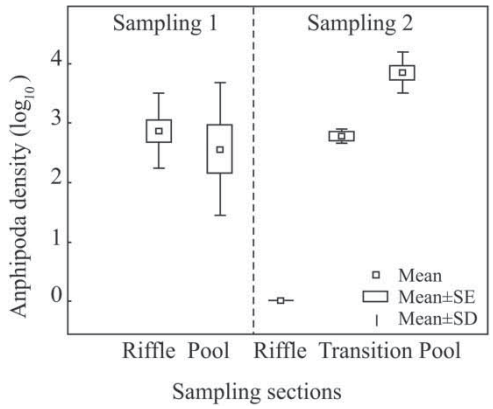

Figure 9 Patterns of Amphipoda population density in riffle, intermediate and pool sections

tendency in density of Amphipoda to increase from riffle to pool at large discharges and to decrease slightly from riffle to pool at small discharges (Fig. 9). It is noteworthy that sampling stations at cross-section 5–5 (left) and cross-section 7–7 (left) were located near the outer bank of the meander with rip-rap protection (Fig. 1). The rip-rap is a stony substrate, which supports largest densities of Amphipoda (Fig. 9).

Quantitatively, the relation between invertebrate densities B and flow characteristics can be found assuming that the bed shear stress $\tau_0 = \rho u_*^2$ and stability of riverbed material, represented by critical bed shear stress $\tau_C = \rho u_C^2$, are the only physical variables that directly and indirectly control the local invertebrate densities:

$$B = F(\tau_0, \tau_C), \text{ or in dimensionless form}$$
$$B = f(\xi),\ \xi = \tau_0/\tau_C \tag{15}$$

where F and f are some functions. Furthermore, assuming that physical interactions between invertebrates and flow at the reach-scale mainly result in migration within the river reach, the dynamics of invertebrate density can be related to migration rate as:

$$\frac{\mathrm{d}B}{B\,\mathrm{d}\xi} = m \tag{16}$$

where m is dimensionless net migration rate. For simplicity other factors of bio-chemical character (reproduction and mortality) are considered to be constant along the entire river reach within meander wavelength. Integration of Eq. (16) with an assumption of constant net migration rate yields:

$$B = B_0 \exp(m\xi) \tag{17}$$

where B_0 is a constant of integration representing the background invertebrate density. Critical shear velocity can be estimated with the use of Shields diagrams (Vanoni, 1975) as $u_{*C} = \sqrt{\tau_C/\rho}$ (Table 4). Using the definition of critical shear velocity, the dimensionless shear stress can be approximated as u_*/u_{*C}.

Table 4 Grain size distribution, critical and actual shear velocities, and group speed of bedform propagation

	Cross-section						
	1	2	3	4	5	6	7
d_{50} (mm)	2.1	1.0	1.5	1.2	2.0	2.3	1.1
			Benthic sampling 1				
u_{*C} (cm s^{-1})	3.7	2.4	3.0	2.6	3.4	3.6	2.5
u_* (cm s^{-1})	1.2	2.2	2.7	1.7	1.7	1.2	2.3
			Benthic sampling 2				
u_{*C} (cm s^{-1})	3.9	2.5	3.3	3.0	4.0	4.3	3.0
u_* (cm s^{-1})	5.5	5.1	5.4	5.8	6.7	6.9	6.5
		Riffle			Pool		
C_1 (cm hr^{-1})		0.5			0.25		
C_2 (cm hr^{-1})		4.2			7.3		

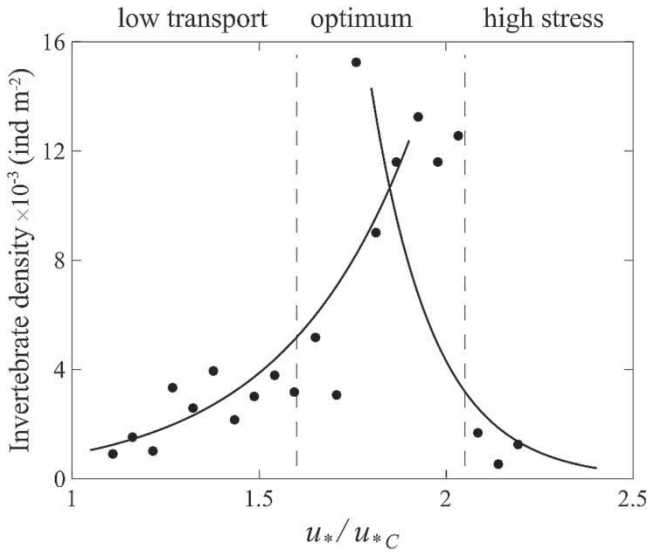

Figure 10 Relations between invertebrate densities and actual and critical shear stress values

The relationship between invertebrate density and u_*/u_{*C} is shown in Fig. 10. Invertebrate density increases exponentially with the increasing u_*/u_{*C} in the range $1 < u_*/u_{*C} < 1.9$ and exponentially decreases with the further increase in u_*/u_{*C}. This suggests that an assumption on constant migration rate is only valid for a limited range of u_*/u_{*C}. Variable migration rate $m = \psi(u_*/u_{*C})$ allows for more complex relations, which will include a combination of hyperbolic tangent and sine functions that would fit better the measured data with an asymmetric bell-shaped function. However, accurate fitting of measured data with an empirical relation is not the goal of this paper, which mainly focuses on the understanding of governing processes. Data in Fig. 10 together with the conceptual model, Eqs (15)–(17), demonstrate that there are three distinct subranges in u_*/u_{*C}: small invertebrate densities at relatively small ratios of u_*/u_{*C}, high invertebrate densities at intermediate u_*/u_{*C}, and low invertebrate densities at large ratios of u_*/u_{*C}. Patterns, similar to that in Fig. 10, are typically observed in ecological studies when performance of organisms is examined in relation to abiotic factors such as temperature. These patterns are usually associated with existence of some optimal range and two subranges with limiting conditions (Cushing & Allan, 2001, 19).

5 Discussion and conclusions

This paper examines spatial and temporal variations in the dynamics of turbulent flow in a natural meander bend of a lowland river and explores the implications of these variations in flow dynamics for the ecology of benthic macro-invertebrates. Previous hydrodynamic research (Sukhodolov, 2012) on the meander bend examined in this study provides detailed information for evaluating numerical hydraulic simulations, which were employed in this research as a tool for exploring spatial and temporal variations in the flow structure.

A quasi three-dimensional Reynolds-Averaged-Navier-Stokes (RANS) numerical model was developed to: (1) explore flow patterns over a range of discharge conditions, and (2) evaluate the velocity reversal hypothesis and its implications for the benthic macro-invertebrates. The results of numerical studies support the velocity reversal hypothesis (Fig. 7). The reversal in the highest magnitude of velocity in the pool versus the riffle occurs at a discharge of about 8 m^3 s^{-1}. At large discharges, with inundation of the floodplain, cross-section averaged velocities in the pool can exceed velocity in the riffle by 1.5 times. This numerical result also supports the conclusion of previous studies that for the velocity reversal to hold in a cross-section average sense, flow continuity requires a difference in the cross-section geometry of riffles and pools at different water levels (Rodríguez, García & García, 2013). Indeed, the cross-sections of the riverbed in the pool demonstrate a triangular shape (wetted area increases with the second power of depth), while the shape of cross-sections in the riffle is close to a rectangular (wetted area increases linearly with depth). Direct measurements of the free-surface slope indicated that the slope increases with increasing water discharge, and this increase is particularly strong in the pool. Together with the increase in characteristic depth scale δ_0, the increase of water surface slope is

responsible for the increase in values of bed shear stress in the pool (Table 2).

In general, the results of hydrodynamics studies in this river reach demonstrate that the variability in cross-section averaged velocity between riffle and pool is about 1.5 fold during high and low flow events. Taking into account that reach-averaged velocity is varying from 0.1 to 0.70 m s^{-1} due to temporal changes in hydraulic regime on the reach, the spatial variability of the flow can be characterized as relatively weak. However, the difference between the structures of flow in the riffle and pool is considerably stronger. Flow in the riffle is less diverse than that in the pool, where, in addition to the patterns of converging/diverging velocity vector fields, it includes secondary currents induced by curvature and flow stagnation near the river banks. Although during events of higher flow the distribution of cross-section averaged characteristics of flow (velocity and bed shear stress) is reversed, the flow structure in the pool becomes even more diverse due to lateral expansion of the counter rotating cells and flow stagnation. This distinguishes the dynamics of flow in bends from the dynamics of straight river reaches with centred riffle-pool sequences, which are characterized by smaller secondary circulation cells (scaling with flow depth) produced by lateral divergence/convergence of velocity vector fields and turbulence anisotropy (Rodríguez, García & García, 2013).

The results of macro-invertebrates surveys indicate a significant variability in the spatial distribution of invertebrates at the meso-scale level. The population density of invertebrates is significantly larger in the pool compared with the riffle (Table 3 and Fig. 8). This observation conforms to the results of previous research in lowland sand-bed streams, which also found significantly higher density of invertebrates in pools than in riffles (McCulloch, 1986). However, Brooks, Haeusler, Reinfelds & Williams (2005), Brown & Brussock (1991) and Quinn & Hickey (1994) reported higher invertebrate density in riffles compared with pools. Moreover, Brooks et al. (2005), Orth & Maughan (1983) and Rempel, Richard & Healey (2000 found that the highest total densities corresponded to locations with low flow velocities. These similarities and differences with past studies indicate the absence of universality in responses of benthic communities to spatial and temporal variability in flow (Lenat, Penrose & Eagleson, 1981), and also illustrate the variety of effects imposed by an increase/reduction in water discharge and velocity as a complex trade-off between flow forcing and food availability. Therefore, in order to interpret the implications of flow dynamics for benthic macro-invertebrates in this study we need to understand the effects of flow on riverbed stability.

Although the locus of maximum velocity in this river reach apparently shifts from the riffle to the pool with increasing stage, the patterns of macro-invertebrates do not appear to mirror this change in flow conditions. In both benthic sampling campaigns the organisms dominated in the pool section. As shown by detailed analysis of flow structure, the pool is not merely a morphological structure, but a biotope with a far more diverse flow structure than the riffle (Figs 2, 3 and 6). More complex hydraulic habitats generally are associated with high population densities (Quinn & Hickey, 1994).

Benthic invertebrates depend strongly on the characteristics of the substrate they colonize. The substrate might be unstable during flooding or silted with fine particulate matter during low flow, although the delivery of fine particulate matter and food resources could be more efficient in that period. Therefore, the implications of flow hydrodynamics should be discussed in the context of stability of the substrate and conditions for deposition/resuspension of fine particulate matter. The stability of riverbed substrate can be examined by comparing actual and critical values of shear velocity. Additionally, the rates of riverbed changes can be characterized by a propagation speed of micro-forms of the riverbed relief with a formula of Snishchenko & Kopaliani (1978) $C = 0.019\,U\,\mathsf{F}^{2.9}$ where C is group speed of bedforms, U is discharge-mean velocity of flow, and F is Froude number (Table 4). The data in Table 4 show that during the sampling 1, the values of measured shear velocities were two to three times smaller than the critical values. The riverbed can be characterized as stable because the propagation of small bed-forms on the riverbed was around few mm per hour. During the flooding, the values of shear velocity exceeded the critical values on average by 1.5 to 2 times and the propagation of bedforms ranged from 4 to 7 cm per hour corresponding to an active migration phase (Kleeberg, Köhler, Sukhodolova & Sukhodolov, 2010). Previous studies on the Spree River also provide useful information on the characteristics of flocculated organic matter transported in suspension. Prochnow et al. (1995) report that particles with settling velocity less than 3×10^{-5} cm s^{-1} comprise up to 60% of the total suspended load. The critical shear velocity for settled flocculated organic matter is about 0.5–1.0 cm s^{-1} (Kleeberg et al., 2010). The settling velocity for mineral particles in the deposits near the river banks ranges from 0.02 cm s^{-1} to 15 cm s^{-1}.

At low flow, the benefits of reduced hydraulic stress for some invertebrates may be counteracted by the negative effects of fine sediment deposition, which reduces habitat complexity by eliminating micro-scale substrate variability produced by coarse sediment. At low flow, fine sediments might accumulate in the river bed and fill interstices that could otherwise provide suitable habitat and refuge from predators (Brown & Brussock, 1991). High inputs of fine sediment to rivers can significantly alter invertebrate assemblages (Wood & Armitage, 1999) and reduce the density of benthic macro-invertebrates (Cobb & Flannagan, 1990; Rutherfold & Mackay, 1986).

During low flow conditions, the riverbed was stable throughout the bend. However, the hydrodynamic conditions in the pools were characterized by smaller values of the shear velocity than values in the riffles. In the pools, the values of shear velocities were roughly equal to the critical values of entrainment of fine particulate matter from the riverbed. This fact indicates that the conditions were more favourable for deposition of organic material/food supply, while slightly coarser substrate ensured

stability. Furthermore, the values of shear velocity were high enough to prevent the silting of the substrate. Therefore, it can be concluded that the variability in hydrodynamics and morphodynamics in the riffle-pool sequence provides the preconditions for observing larger population densities of macro-invertebrates in the pool area.

Conventionally, substrate instability is associated with a reduction in population density of organisms (Cobb, Galloway & Flannagan, 1992; Death & Winterbourn, 1995). During high flow, when the water level was still within the river channel (benthic sampling 2), the hydrodynamic conditions in the riffles and pools were reversed, although the magnitudes of shear velocity were too small to change significantly the stability of the substrate. The high shear velocities produced increased rates of bed-forms propagation but the propagation rates were in the range of few cm per hour, hence providing macro-invertebrates with enough time to adjust to changing bed conditions. We suggest that the range of shear velocity from 5.1 to 6.9 cm s^{-1} is strong enough to cause a sweep of fine sediments (silt and clay) from the sediment grain interstices, that invertebrates can then inhabit. When the bed shear stress is further increased, macro-invertebrates might be involved in uncontrollable or catastrophic drift (Giller & Malmqvist, 1998).

There are few studies linking the propagation speed of bed-forms and invertebrates distribution patterns. A study conducted in the Paraná River (Amsler, Blettler & Ezcurra de Drago, 2009) shows a preference for invertebrates to inhabit places with a moderate speed of migration of superimposed dunes (40–80 cm hr^{-1}), and a tendency for macro-invertebrate densities to decrease when propagation speeds exceed these values. The high speed of propagation is not comparable with the values found herein (Table 4), but it indicates that the effect of substrate stability is related to the species adaptations and river scales, and, like the effect of flow fluctuation on benthic fauna, it is not a universal phenomenon. Nevertheless, the difference in the propagation speed of the bed-forms can have significant implications and can explain the larger population density of Oligochaeta (*Naididae*) and Bivalvia in the riffle during the flooding.

For other invertebrate groups, like Amphipoda, the composition of the substrate plays a key role in selection of habitat during the high flow events. *C. curvispinum* is a Ponto-Caspian invader species and it is associated with the clumps of another Ponto-Caspian invader, *Dreissena polymorpha* (Jażdżewski & Konopacka, 2002). The shells of these invertebrates offer a solid base for building silt tubes, which are inhabited by this amphipod, and like a refuge protect invertebrates against stronger currents (Grabowski, Jazdzewski & Konopacka, 2007). It might also explain why these invertebrates can inhabit the areas with larger shear velocities, such as for instance, the pool during the flooding (Fig. 9). In fact, shells were abundant in the composition of the riverbed material in the pool sections. Besides, *C. curvispinum* builds mud tubes on the stony substrates resulting in changes in the relief of the riverbed (Haas, Brunke & Strei, 2002). This, in turn, creates inter-tube spaces particularly suitable for the development of communities composed of gammarids (including *D. haemobaphes*), oligochaetes, leeches, bivalves, and chironomids (Lubyanov, Buzakova & Gaydash, 1967). The fact that shells of *D. polymorpha* were not found in the riffle during benthic sampling 2 could help explain why no amphipods were collected there (Fig. 9). However, this observation consisted only of visual inspection of the riverbed samples and the quantitative analysis of the content was not performed.

The results of this study are summarized as follows:

- This case study demonstrates how spatial heterogeneity of riverbed morphology and secondary flow induced by channel curvature together with flow stagnation along the banks make pools hydraulically more diverse compared with riffles. It also explores how complex geometry in this meander bend produces temporal variations on spatially variable flow due to velocity reversal between riffles and pools.
- Patterns of macro-invertebrates indicate an increase in population density from riffle to pool, following the increase in diversity of abiotic factors. For most invertebrate species the observed patterns persisted during temporal variations in flow. Theoretical analysis for the relations between flow characteristics and invertebrate densities, introduced in this study, indicates that an optimal range of hydraulic conditions and substrate characteristics are the key factors defining observed responses of invertebrate communities.

Acknowledgements

The authors are thankful to N. Nikolaevich for assistance in field measurements. J. Kaschtschejewa helped with the data post-processing and preparing illustrations. Bruce Rhoads and two anonymous reviewers are thanked for their constructive criticism and detailed and helpful comments.

Funding

This work was partly supported by Deutscher Akademischer Austausch Dienst [DAAD, grant A0873748], Deutsche Forschungsgemeinschaft [DFG, grants SU 405/4, SU 405/7], National Natural Science Foundation of China [grant number 10702042], and the Shanghai Leading Academic Discipline Project [Project Number B206].

Notation

g = gravity acceleration (m s^{-2})
F = Froude number (–)
H = cross-section averaged flow depth (m)
h = local flow depth (m)
Q = water discharge (m^3 s^{-1})
$q_{x,y,z}$ = specific discharge ($m^2 s^{-1}$)

R = Reynolds number (–)
R = radius of curvature (m)
S_θ = longitudinal slope of the free surface (–)
S_r = radial slope of the free surface (–)
U = cross-section averaged flow velocity (m s^{-1})
$\overline{u}$ = local depth-averaged velocity (m s^{-1})
u_θ = mean tangential velocity (m s^{-1})
u'_θ = fluctuation of tangential velocity (m s^{-1})
u_r = mean radial velocity (m s^{-1})
u'_r = fluctuation of radial velocity (m s^{-1})
u = mean streamwise velocity (m s^{-1})
v = mean transverse velocity (m s^{-1})
w = mean vertical velocity (m s^{-1})
w' = fluctuation of vertical velocity (m s^{-1})
u_* = shear velocity (m s^{-1})
y = lateral distance (m)
z = distance from the riverbed (m)
z_0 = hydrodynamic roughness length (m)
ζ, ζ^* = dimensionless coordinates (–)
η = dimensionless coordinate (–)
κ = von Kármán constant (–)
ν_t = turbulent viscosity ($m^2 s^{-1}$)
τ = shear stress (N m^{-2})
ρ = water density (kg m^{-3})
σ = dimensionless vertical coordinate (–)
ϑ = dimensionless coefficient (–)
δ = vertical length scale (m)
δ_0 = modified characteristic length scale (m)

References

Abad, J. D., & Garcia, M. H. (2009). Experiments in a high-amplitude Kinoshita meandering channel: 1. Implications of bend orientation on mean and turbulent flow structure. *Water Resources Research*, *45*, W02401.

Abad, J. D., Frias, C., Garcia, M., & Buscaglia, G. (2013). Modulation of the flow structure by progressive bedforms in the Kinoshita meandering channel. *Earth Surface Processes & Landforms*, *38*, 1612–1622.

Anwar, H. O. (1986). Turbulent structure in a river bend. *Journal Hydraulic Engineering*, *112*, 657–669.

Amsler, M., Blettler, M., & Ezcurra de Drago I. (2009). Influence of hydraulic conditions over dunes on the distribution of the benthic macro-invertebrates in a large sand bed river. *Water Resources Research*, *45*, WO6426.

Bathurst, J. C. (1982). Channel bars in gravel-bed rivers [Discussion]. In R. D. Hey, J. C. Bathurst, & C. R. Thorne (Eds.), *Gravel-bed rivers* (pp. 330–331). Chichester: Wiley.

Bathurst, J. C., Thorne, C. R., & Hey, R. D. (1979). Secondary flow and shear stress at river bends. *Journal Hydraulic Division American Society of Civil Engineers*, *105*, 1277–1713.

Blanckaert, K., & de Vriend, H. J. (2003). Nonlinear modeling of mean flow redistribution in curved open channels. *Water Resources Research*, *39*, W01375.

Blettler, M., Amsler, M., Ezcurra de Drago I., & Marchese, M. (2008). Effects of stream hydraulics and other environmental variables on density of benthic macroinvertebrates in the Paraná River system. *River Research and Applications*, *24*, 1124–1140.

Blettler, M., Sukhodolov, A., & Tockner, K. (2010). Hydraulic conditions over bed forms control the benthic fauna distribution in a lowland river (Spree River, Germany). In A. Dittrich, K. Koll, J. Aberle & P. Geisenhainer (Eds.), *River flow 2010. Proceedings of the Fifth International Conference on Fluvial Hydraulics*, 7–10 September 2010, Braunschweig, Germany, *2*, 1463–1467.

Blumberg, A. F., & Mellor, G. L. (1983). Diagnostic and prognostic numerical circulation studies of the South Atlantic Bight. *Journal of Geophysical Research*, *88*, 4579–4592.

Brooks, A. J., Haeusler, T., Reinfelds, I., & Williams, S. (2005). Hydraulic microhabitats and the distribution of macroinvertebrate assemblages in riffles. *Freshwater Biology*, *50*, 331–344.

Brown, A. V., & Brussock, P. P. (1991). Comparisons of benthic invertebrates between riffles and pools. *Hydrobiologia*, *220*, 99–108.

Callaghan, F. M., Cooper, G. G., Nikora, V. I., Lamouroux, N., Statzner, B., Sagnes, P., Radford, J., Malet, E., & Biggs, B. J. (2007). A submersible device for measuring drag forces on aquatic plants and other organisms. *New Zealand Journal Marine and Freshwater Research*, *4*, 119–127.

Carling, P. A. (1995). Implications of sediment transport for instream flow modelling of aquatic habitat. In D. M. Harper & A. J. A. Ferguson (Eds.), *The ecological basis for river management* (pp. 17–31). Chichester: Wiley.

Casulli, V., & Cattani, E. (1994). Stability, accuracy and efficiency of a semi-implicit method for three-dimensional shallow water flow. *Computers and Mathematics with. Applications*, *27*, 99–112.

Chen, X. J. (2003). A non-hydrostatic model for three-dimensional free-surface flows. *International Journal of Numerical Methods in Fluids*, *42*, 929–952.

Cobb, D. G., & Flannagan, J. F. (1990). Trichoptera and substrate stability in the Ochre River, Manitoba. *Hydrobiologia*, *206*, 29–38.

Cobb, D. G., Galloway, T. D., & Flannagan, J. F. (1992). Effects of discharge and substrate stability on density and species composition of stream insects. *Canadian Journal of Fisheries and Aquatic Sciences*, *49*, 1788–1795.

Cushing, C. E., & Allan, J. D. (2001). *Streams. Their ecology and life* (p. 366). San Diego, CA: Academic Press.

Davies, A. M., Jones, J. E., & Xing, J. (1997). Review of recent developments in tidal hydrodynamic modeling, I: Special models. *Journal of Hydraulic Engineering*, *123*, 278–290.

Death, R. G., & Winterbourn, M. J. (1995). Diversity patterns in stream benthic invertebrate communities: The influence of habitat stability. *Ecology*, *76*, 1446–1460.

Degani, G., Herbst, G. N., Ortal, R., Bromley, H. J., Netzer, Y, & Glanman, H. (1993). Relationship between current velocity, depth, and the invertebrate community in a stable river system. *Hydrobiologia*, *263*, 163–172.

Dietrich, W. E., & Smith, J. D. (1983). Influence of the point-bar on flow through curved channels. *Water Resources Research*, *19*, 1173–1192.

Doledec, S., Lamouroux, N., Fuchs, U., & Merigoux, S. (2007). Modelling the hydraulic preferences of benthic macroinvertebrates in small European streams. *Freshwater Biology*, *52*, 145–164.

Engel, F. L., & Rhoads, B. L. (2012). Interaction among mean flow, turbulence, bed morphology, bank failures and channel planform in an evolving compound meander loop. *Geomorphology*, *163*, 70–83.

Engelund, F. (1974). Flow and topography in channel bends. *Journal of Hydraulic Divivison American Society of Civil Engineers*, *100*, 1631–1648.

Fuller, R. L., & Mackay, R. J. (1981). Effects of food quality on growth of three *Hydropsyche* species (Trichoptera: Hydropsychidae). *Canadian Journal of Zoology*, *59*, 1133–1140.

Frothingham, K. M., & Rhoads, B. L. (2003). Three-dimensional flow structure and channel change in an asymmetrical compound meander loop, Embarras River, Illinois. *Earth Surface Processes and Landforms*, *28*, 625–644.

Gibbins, C., Verticat, D., & Batulla, R. J. (2007). When is stream invertebrates drift catastrophic? The role of hydraulics and sediment transport in initiating drift during flood events. *Freshwater Biology*, *52*, 2369–2384.

Giller, P. S., & Malmqvist, B. (1998). *The biology of streams and rivers*. Oxford: Oxford University Press.

Grabowska, J., & Grabowski, M. (2005). Diel-feeding activity in early summer of racer goby Neogobius gymnotrachelus (Gobiidae): A new invader in the Baltic basin. *Journal of Applied Ichtyology*, *21*, 282–286.

Grabowski, M., Jazdzewski, K., & Konopacka, A. (2007). Alien Crustacea in Polish waters – Amphipoda. *Aquatic Invasions*, *2*, 25–38.

Haas, G., Brunke, M., & Strei B. (2002). Fast turnover in dominance of exotic species in the Rhine River determines biodiversity and ecosystem function: An affair between amphipods and mussels. In E. Leppäkoski, S. Gollasch & S. Olenin (Eds.), *Invasive aquatic species of Europe: Distribution, impacts and management* (pp. 426–432). Dordrecht: Kluwer Academic.

Hart, D. D., Clark, B. D., & Jasentuliyana, A. (1996). Fine-scale field measurement of benthic flow environments inhabited by stream invertebrates. *Limnology & Oceanography*, *41*, 297–308.

Hart, D. D., & Merz, R. A. (1998). Predator-prey interactions in benthic stream community: A field test of flow-mediated refuges. *Oecologia*, *114*, 263–273.

Holomuzki, J. R., & van Loan, A. S. (2002). Effects of structural habitat on drift distance and benthic settlement of the caddisfly Ceratopsy sparna. *Hydrobiologia*, *477*, 139–147.

Ippen, A. T., Drinker, P. A., Jobin, W. R., & Shemdin, O. H. (1962). Stream dynamics and boundary shear distributions for curved trapezoidal channels. *MIT Hydrodynamic Laboratory Report*, *47*.

Jackson, R. G. (1975). Velocity-bed-form-texture patterns of meander bends in the lower Wabash River of Illinois and Indiana. *Bulletin of Geological Society of America*, *86*, 1511–1522.

Jażdżewski, K., & Konopacka, A. (2002). Invasive Ponto-Caspian species in waters of the Vistula and Oder basins and the southern Baltic Sea. In E. Leppäkoski, S. Gollasch, S. Olenin (Eds.), *Invasive aquatic species of Europe – distribution, impacts and management* (pp. 384–398). Dordrecht: Kluwer Academic.

Jowett, I. G. (1993). A method for objectively identifying pool, run and riffle habitats from physical measurements. *New Zealand Journal of Marine and Freshwater Research*, *27*, 241–248.

Kawamura, S., Hasegawa, K., & Yuping, Z. (2003). Hydraulic environment feature of step-pool systems and habitat of benthos a case in the Gunbetsu River. Third IAHR Symposium on *River*, *Coastal and Estiarine Morphodynamics*. Barcelona, Spain.

Keller, E. A. (1971). Areal sorting of bed-load material: The hypothesis of velocity reversal. *Bulletin of Geological Society of America*, *82*, 753–756.

Keller, E. A., & Florsheim, J. L. (1993). Velocity-reversal hypothesis: A model approach. *Earth Surface Processes and Landforms*, *18*, 733–740.

Kleeberg, A., Köhler, J., Sukhodolova, T., & Sukhodolov, A. (2010). Effects of aquatic macrophytes on organic matter deposition, resuspension and phosphorus entrainment in a lowland river. *Freshwater Biology*, *55*, 326–345.

Leopold, L. (1996). *A view of the river*. Cambridge, MA: Harvard University Press.

Lenat, D. R., Penrose, D. L., & Eagleson, K. W. (1981). Variable effects of sediment addition on stream benthos. *Hydrobiologia*, *79*, 187–194.

Lloyd, F., & Sites, R. W. (2000). Microhabitat associations of three species of Dryopidea (Coleoptera) in Ozark stream: A comparison of substrate, and simple and complex hydraulic characters. *Hydrobiologia*, *439*, 103–114.

Lubyanov, I. P., Buzakova, A. M., & Gaydash, Y. K. (1967). Changes in composition of macro- and microzoobenthos of the Dneprovskoe Reservoir after establishment of regulated run-off in the middle course of the Dnieper River. In K. S. Vladimirova, K. K. Zerov, G. L. Melnichuk, G. A. Olivari,

Y. Y. Tseeb (Eds.), *Hydrobiological regime of the Dnieper River under conditions of regulated run-off* (pp. 167–175). Kiev: Naukova Dumka Press.

MacWilliams, M. L. Jr, Wheaton, J. M., Pasternack, G. B., Street, R. L., & Kitanidis, P. K. (2006). Flow convergence routing hypothesis for pool-riffle maintenance in alluvial rivers. *Water Resources Research*, *42*, W10427.

Malmqvist, B., & Sackmann, G. (1996). Changing risk of predation for a filter-feeding insect along a current velocity gradient. *Oecologia*, *108*, 450–458.

McCulloch, D. L. (1986). Benthic macroinvertebrate distributions in the riffle-pool communities of two east Texas streams. *Hydrobiologia*, *135*, 61–70.

McNair, J. N., Newbold, J. D., & Hart, D. D. (1997). Turbulent transport of suspended particles and dispersing benthic organisms: How long to hit bottom? *Journal of Theoretical Biology*, *188*, 29–52.

Nanson, R. A. (2010). Flow fields in tightly curving meander bends of low width-depth ratio. *Earth Surface Processes and Landforms*, *35*, 119–135.

Newson, M. D., & Newson, C. L. (2000). Geomorphology, ecology and river channel habitat; mesoscale approaches to basin-scale challenges. *Progress in Physical Geography*, *24*, 195–217.

Nezu, I., & Nakagawa, H. (1993). *Turbulence in open-channel flows*. Rotterdam: A. Balkema.

Nikolaevich, N., Sukhodolov, A., & Engelhardt, C. (2004). Assaying historical maps and relict channel forms for the analysis of channel processes (on example of the Spree River in Germany). In M. Greco et al. (Eds.), *RiverFlow 2004: Proceedings of the international congress on fluvial hydraulics 1* (pp. 181–189). Rotterdam: A. Balkema.

Orth, D. J., & Maughan, E. (1983). Microhabitat preferences of benthic fauna in a woodland stream. *Hydrobiologia*, *106*, 157–168.

Padmore, C. L. (1997). *Physical biotopes in representative river channels: identification, hydraulic characterisation and application* (PhD thesis). Department of Geography, University of Newcastle, Newcastle-upon-Tyne.

Padmore, C. L. (1998). The role of physical biotopes in determining the conservation status and flow requirements of British rivers. *Aquatic Ecosystems Health Management*, *1*, 25–35.

Powers, S. P, & Kittinger, J. N. (2002). Hydrodynamic mediation of predator-prey interactions: Differential patterns of prey susceptibility and predator success explained by variation in water flow. *Journal Experimental Marine Biology and Ecology*, *273*, 171–187.

Prochnow, D., Bungartz, H., Engelhardt, C., Freidrich, H.-J., Krueger, A., Lueder, A., Sauer, W., Schild, R., & Thiele, M. (1995). Quantitative Erfassung, Modellirung und Simulation der Ausbreitung von gekoppelten Schweb-und Schadstofffractionen in flachen Gewaessern, Forschungsbericht PR 400/1-1, Berlin.

Quinn, J. M., & Hickey, C. W. (1994). Hydraulic parameters and benthic invertebrate distributions in two gravel-bed New Zealand rivers. *Freshwater Biology*, *32*, 489–500.

Rempel, L. L., Richard, J. S., & Healey, M. C. (2000). Macroinvertebrates community structure along gradients of hydraulic and sedimentary conditions in a large gravel-bed river. *Freshwater Biology*, *45*, 57–73.

Rhie, C. M., & Chow, W. L. (1983). Numerical study of the turbulent flow past an airfoil with trailing edge separation. *AIAA Journal*, *21*, 1525–1532.

Rhoads, B. L., & Massey, K. D. (2012). Flow structure and channel change in a sinous grass-lined stream within an agriculatural drainage ditch: Implications for ditch stability and aquatic habitat. *River Research and Applications*, *28*, 39–52.

Rodríguez, J. F., García, C. M., & García, M. H. (2013). Three-dimensional flow in centered pool-riffle sequence. *Water Resources Research*, *49*, 202–215.

Rozovskii, I. L. (1957). *Flow of water in bends of open-channels*. Kiev: Academy of Sciences of Ukraine.

Rutherfold, J. E., & Mackay, R. J. (1986). Patterns of pupal mortality in field populations of *Hydropsyche* and *Cheumatopsyche* (Trichoptera: Hydropsychidae). *Freshwater Biology*, *16*, 337–350.

Sagnes, P., Merigoux, S., & Peru, N. (2008). Hydraulic habitat use with respect to body size of aquatic insect larvae: Case of six species from a French Mediterranean type stream. *Limnologica – Ecology and Management of Inland Waters*, *38*, 23–33.

Schnauder, I., & Sukhodolov, A. (2012). Flow in a tightly curved meander bend: Effects of seasonal changes in aquatic macrophyte cover. *Earth Surface Processes and Landforms*, *37*, 1142–1157.

Sear, D. A. (1986). Sediment transport in pool-riffle sequences. *Earth Surface Processes and Landforms*, *21*, 241–262.

Shapiro, S. S., & Wilk, M. B. (1965). An analysis of variance test for normality (complete samples). *Biometrika*, *52*, 591–611.

Spalart, P. R. (2000). Strategies for turbulence modelling and simulations. *International Journal of Heat and Fluid Flow*, *21*, 252–263.

Snishchenko, B. F., & Kopaliani, Z. D. (1978). Sand wave formation due to irregular bed load motion. *Mechanics of Sediment Transport, Equmec Colloquium*, *156*, 109–117.

Sokal, R. R., & Rohlf, F. J. (1981). *Biometry*. 2nd ed. San Francisco, CA: Freeman.

Stølum, H.-H. (1998). Planform geometry and dynamics of meandering rivers. *Bulletin of Geological Society of America*, *110*, 1485–1498.

Sukhodolov, A. (2012). Structure of turbulent flow in a meander bend of a lowland river. *Water Resources Research*, *47*, W01516.

Sukhodolov, A., & Uijttewaal, W. S. J. (2010). Assessment of a river reach for environmental fluid dynamics studies. *Journal Hydraulic Engineering*, *136*, 880–888.

Teleki, P. G. (1972). Areal sorting of bed-load material: The hypothesis of velocity reversal [Discussion]. *Bulletin of Geological Society of America*, *83*, 911–914.

Termini, D., & Greco, M. (2006). Computation of flow velocity in rough channels. *Journal of Hydraulic Research*, *44*, 777–784.

Thorne, C. R., Zevenbergen, L. W., Pitlick, J. C., Rais, S., Bradley, J. B., & Julien, P. Y. (1985). Direct measurements of secondary currents in a meandering sand-bed river. *Nature*, *316*, 746–747.

van der Velde, G., Rajagopal, S., van den Brink, F. W. B., Kelleher, B., Paffen, B. G. P., Kempers, A.J., & Bij de Vaate, A. (1998). Ecological impact of an exotic invasion in the River Rhine. In P. H. Nienhuis, R. S. E. W. Leuven, & A. M. J. Ragas (Eds.), *New concepts for sustainable management of river basins* (pp. 159–169). Leiden: Backhuys.

Vanoni, V. A. (1975). *Sedimentation engineering. Manuals and reports of engineering practice*, *54*. New York: ASCE.

van Riel, M. C., Van der Velde, G., Rajagopal, S., Marguillier, S., Dehairs, F., & de Vaate, A. (2006). Trophic relationships in the Rhine food web during invasion and after establishment of the Ponto-Caspian invader *Dikerogammarus villosus*. *Hydrobiologia*, *565*, 39–58.

Wadeson, R. A. (1994). A geomorphological approach to the identification and classification of instream flow environment. *South Africa Journal of Aquatic Research*, *20*, 38–61.

Wetmore, S. H., Mackay, R. J., & Newbury, R. W. (1990). Characterization of the hydraulic habitat of brachycentrus-occidentalis a filter-feeding caddisfly. *Journal of North American Benthic Society*, *9*, 157–169.

Wilcox, A. C., Peckarsky, B. L., Taylor, B. W., & Encalada, A. C. (2008). Hydraulic and geomorphic effects on mayfly drift in high-gradient streams at moderate discharges. *Ecohydrology*, *1*, 176–186.

Wood, P. J., & Armitage, P. D. (1999). Sediment deposition in a small lowland stream: Management implications. *Regulated Rivers Research and Management*, *15*, 199–210.

Zeng, J., Constantinescu, G., Blanckaert, K., & Weber, L. (2008). Flow and bathymetry in sharp open-channel bends: Experiments and predictions. *Water Resources Research*, *44*, W09401.

Zhang, J. X., Liu, H., & Xue, L. P. (2006). A vertical 2-D mathematical model for hydrodynamic flows with free surface in σ coordinate. *Journal of Hydrodynamics B*, *18*, 82–90.

Zhang, Q. Y., & Chan, E. S. (2003). Sensitivity studies with the three-dimensional multi-level model for tidal motion. *Ocean Engineering*, *30*, 1489–1505.